

# Structural precursor to freezing: An integral equation study

Joseph M. Brader

*Fachbereich Physik, Universität Konstanz, D-78457 Konstanz, Germany*

(Dated: October 23, 2018)

## Abstract

Recent simulation studies have drawn attention to the shoulder which forms in the second peak of the radial distribution function of hard-spheres at densities close to freezing and which is associated with local crystalline ordering in the dense fluid. We address this structural precursor to freezing using an inhomogeneous integral equation theory capable of describing local packing constraints to a high level of accuracy. The addition of a short-range attractive interaction leads to a well known broadening of the fluid-solid coexistence region as a function of attraction strength. The appearance of a shoulder in our calculated radial distribution functions is found to be consistent with the broadened coexistence region for a simple model potential, thus demonstrating that the shoulder is not exclusively a high density packing effect.

PACS numbers: 61.20.Gy, 61.20.Ne, 05.20.Jj

## I. INTRODUCTION

The hard-sphere system has been of central interest in the theory of fluids since the early work of Boltzmann and is still an important model system in statistical physics. At low and intermediate densities the equilibrium pair structure and thermodynamics are theoretically well understood and the model can be regarded as solved, in the sense that the numerical results agree with simulation to an accuracy satisfactory for most applications. At high density the system undergoes a first-order liquid-solid transition to an FCC crystal<sup>1,2</sup> the theoretical description of which remains an open problem. The challenge for theoretical treatments of the freezing transition is to obtain a unified description of both the amorphous fluid and the symmetry broken solid. The density functional theory of freezing provides a pragmatic approach to this problem in which the solid is regarded as a highly inhomogeneous fluid<sup>3</sup>. By employing a separate treatment of the fluid and solid branches of the free energy (crystal symmetry is input to the theory by hand) modern density functional approximations are able to locate the coexisting densities of the hard-sphere freezing transition in close agreement with simulation<sup>4,5</sup>. Nevertheless, a unified theory in which the crystal symmetry emerges spontaneously upon increasing the density is still lacking.

One possible method of gaining insight into the emergence of crystalline order is to investigate in detail the microscopic structure of the fluid state at densities close to, but below, the freezing transition. Recent simulations performed within this density range suggest the existence of precursor structures to freezing in the high density liquid state of hard-spheres in two and three-dimensions. It has been demonstrated<sup>6</sup> using molecular dynamics simulations that the radial distribution function (RDF) of both the hard-disk and hard-sphere systems develops a shoulder feature in the second peak which first appears at packing fractions within roughly five percent of their respective freezing transitions. To facilitate visualization of configurations the analysis focused primarily on the hard-disk system for which a signature four-particle hexagonal-close-packed configuration of disks was identified as being responsible for the observed shoulder in the RDF. This distinct structural motif reflects the next-nearest-neighbour ordering of the hexagonal domains which develop as the density is increased towards freezing. An analogous scenario was also proposed for the hard-sphere system but not analyzed in detail. A careful simulation study of the three-dimensional case<sup>7</sup> revealed six-membered ring configurations which flatten and increase in frequency close to

freezing were identified as the relevant structural motif responsible for the shoulder observed in the simulation RDF. The existence of the shoulder has long been recognized and exploited by simulators as an empirical indicator for crystallization in hard particle systems, enabling expensive free-energy calculations to be avoided. As a result of the recent simulation studies<sup>6,7</sup> the microscopic origin of this feature is now understood. Considering more general interparticle interactions, it is natural to inquire whether similar precursor structures also occur in systems with an attractive component to the pair potential. In particular, hard-spheres with short-range attraction present a liquid-solid coexistence region which broadens dramatically with increasing attraction strength, leading to coexistence between low-density fluid and high-density solid phases. The possible existence of local crystalline ordering at statepoints in the vicinity of this more general freezing boundary remains to be investigated and raises the question whether the RDF shoulder may also be present at low density statepoints far removed from the hard-sphere transition point.

The most powerful theoretical technique for calculating the pair correlations and thermodynamics of classical fluids in equilibrium is the method of integral equations, formed by approximate closures of the Ornstein-Zernike equation<sup>8,9</sup>. For many model interaction potentials integral equations provide highly accurate structural information at low and intermediate coupling strength (although difficulties do remain in the vicinity of critical points, when they occur<sup>10</sup>). It is therefore surprising that none of the regularly applied integral equation theories for the pair structure are capable of describing the RDF shoulder of hard-spheres and miss completely this well established feature of the equilibrium fluid pair structure, despite their admirable success at fluid statepoints removed from freezing. This failure raises the fundamental question whether the method of integral equations is capable, either in practice or in principle, of indicating the existence of a fluid-solid transition. Finding an integral equation theory which can correctly predict from first principles the detailed structure of the RDF in the high density liquid may thus shed some light on this important theoretical question<sup>11</sup>.

In this paper we address the issue of precursor structures using inhomogeneous integral equation theory. This class of theory is based upon the inhomogeneous Ornstein-Zernike equation<sup>3,8</sup> in combination with closure relations between the inhomogeneous direct and total correlation functions. In contrast to their homogeneous counterparts, which involve relations between pair functions, inhomogeneous integral equation theories work at the level

of the triplet correlations. As the problem of crystallization and the appearance of precursor structures is associated with an increased local orientational ordering in the system, it is reasonable to suppose that increasing the orientational resolution of the theoretical treatment, i.e. working at the triplet rather than the pair level, will better capture the relevant physics. While a general theory of the emergence of crystalline order is still highly desirable (and we make no claims to provide this) we demonstrate that inhomogeneous integral equation theory predicts the occurrence of an RDF shoulder in the vicinity of freezing and thus yields indirect evidence for the existence of underlying precursor structures. By considering purely equilibrium fluid statepoints below the freezing transition we avoid the potential complications associated with metastable states.

The remainder of the paper will be structured as follows: In Section II we outline the phenomenology of the shoulder in the hard sphere RDF as found in simulation, briefly review existing integral equation approaches and introduce the inhomogeneous integral equation theory to be employed in this work. In Section III A we present numerical solutions of the inhomogeneous theory for hard spheres and compare these with simulation data. In Section III B we consider the influence on the RDF of adding a short-range attraction to the hard-sphere pair potential. Finally, in Section IV we will discuss our results and give an outlook for future work.

## II. THEORETICAL APPROACHES

The simulation results of Truskett *et al*<sup>6</sup> show that in both two and three-dimensions the shoulder in the simulation RDF first becomes apparent within approximately five percent of the freezing transition. For the purpose of the present work we restrict ourselves to the case of three-dimensional hard-spheres for which the relevant density range is  $0.47 < \eta < 0.494$ . The packing fraction is given by  $\eta = \pi\rho\sigma^3/6$  for given number density  $\rho$  and we take the sphere diameter  $\sigma$  as the unit of length. In Figure.1 we show the RDF obtained from Monte-Carlo simulation for  $\eta = 0.494$ <sup>12</sup>, where the shoulder is most distinct, together with that of the hard-sphere solid at the melting point, located at  $\eta = 0.545$ <sup>13</sup>. Within the high density fluid there exist ordered crystalline domains with a local structure similar to that of the solid phase at the melting point and which lend a significant statistical weight to the RDF<sup>6</sup>. Comparison of the coexisting fluid and solid structure in Figure.1 is indeed suggestive of

local crystalline ordering. The fluid phase RDF is enhanced (suppressed) around the peaks (troughs) of the coexisting solid RDF relative to what would be expected on the basis of a simple extrapolation of the intermediate density fluid RDF up to freezing. The inset to Figure.1 shows more clearly the detailed structure of the second peak at freezing, in particular the shoulder which approximately spans the range  $1.73 < r < 1.95$ .

The most commonly used theories of the pair structure of classical fluids in equilibrium are based upon closures of the Ornstein-Zernike equation<sup>8</sup>

$$h(r_{12}) = c(r_{12}) + n \int d\mathbf{r}_3 c(r_{13}) h(r_{32}), \quad (1)$$

where  $n$  is the bulk density and  $h(r) = g(r) - 1$ . Eq.(1) serves to define the direct correlation function  $c(r)$  which is a function of simpler structure and shorter range (for finite range potentials) than  $h(r)$ . When supplemented by an independent relation between  $h(r)$  and  $c(r)$ , containing the details of the interaction potential, (1) yields a closed integral equation for the pair correlations in the system. Integral equation theories are non-perturbative in character and, although the approximations involved are largely uncontrolled, can produce excellent results for some model fluids. The classic closure approximations are the Percus-Yevick (PY)<sup>14</sup> and Hyper-Netted-Chain (HNC)<sup>15</sup>, both of which can be systematically derived using diagrammatic techniques<sup>16</sup>. For hard-spheres these theories have been subsequently improved upon by closures such as the Generalized-Mean-Spherical-Approximation (GMSA)<sup>17</sup>, Martynov-Sarkisov<sup>18</sup>, Ballone-Pastore-Galli-Gazzillo<sup>19</sup>, Verlet-Modified<sup>20</sup>, Rogers-Young<sup>21</sup> and Modified-Hyper-Netted-Chain<sup>22</sup>. Although these improved theories represent the state of the art in the theory of fluids, none of them captures the shoulder in the RDF close to freezing<sup>23</sup>. In the inset to Figure.1 we show a representative example of this failure by comparing the GMSA theory with simulation at freezing. The triangular structure of the second peak from the GMSA theory is typical of integral equation theories based on (1), missing both the detailed structure of the second peak and incorrectly predicting both the location and depth of the first minimum. For  $\eta < 0.45$  all of the above mentioned theories are reliable and agree with simulation data to an acceptable level of accuracy.

The primary advance of the theories described above is to improve the thermodynamic output with respect to the PY and HNC closures by treating more accurately the RDF in the vicinity of contact. This is typically achieved by incorporating an additional parameter into the theory which can be determined by requirements of thermodynamic consistency.

At statepoints removed from freezing this appears to be quite adequate and leads to a good description of the pair correlations at all separations. In order to capture the high density shoulder a treatment which describes more accurately local packing effects is required. A natural extension of approaches based on (1) is to use instead the inhomogeneous Ornstein-Zernike equation<sup>3,8</sup> as a starting point and consider closure relations between the inhomogeneous direct and total correlation functions,  $c(\mathbf{r}_1, \mathbf{r}_2)$  and  $h(\mathbf{r}_1, \mathbf{r}_2)$ . The inhomogeneous Ornstein-Zernike equation is given by

$$h(\mathbf{r}_1, \mathbf{r}_2) = c(\mathbf{r}_1, \mathbf{r}_2) + \int d\mathbf{r}_3 c(\mathbf{r}_1, \mathbf{r}_3) n(\mathbf{r}_3) h(\mathbf{r}_3, \mathbf{r}_2), \quad (2)$$

where  $n(\mathbf{r})$  is the spatially varying density in the presence of an arbitrary external field. In the absence of an external potential the system is translationally invariant,  $c(\mathbf{r}_1, \mathbf{r}_2) \rightarrow c(r_{12})$  and  $h(\mathbf{r}_1, \mathbf{r}_2) \rightarrow h(r_{12})$ , and we recover (1). As the inhomogeneous one and two-body distribution functions exhibit the same symmetries as the external potential it is possible to simplify (2) using integral transforms for the special cases of an external potential possessing either planar or spherical symmetry. In planar geometry Hankel transformation reduces (2) to a one-dimensional integral<sup>24</sup>. This simplification has enabled application of inhomogeneous Ornstein-Zernike theory to both adsorption at planar substrates and the liquid-vapour interface<sup>25</sup>. In spherical geometry the factorization of (2) is achieved using Legendre transforms<sup>26</sup>. An arbitrary spherically inhomogeneous function  $f(\mathbf{r}_1, \mathbf{r}_2)$  can be expressed as a function of two scalar radial variables,  $r_1$  and  $r_2$ , and the cosine of the angle between them,  $x_{12} \equiv \cos(\theta_{12})$ . The Legendre transform is thus given by

$$\hat{f}_n(r_1, r_2) = \frac{2n+1}{2} \int_{-1}^1 dx_{12} f(r_1, r_2, x_{12}) P_n(x_{12}), \quad (3)$$

where  $P_n(x)$  is the Legendre polynomial of degree  $n$ . The inverse transform is given by

$$f(r_1, r_2, x_{12}) = \sum_{n=0}^{\infty} \hat{f}_n(r_1, r_2) P_n(x_{12}). \quad (4)$$

The practical advantage of using Legendre transforms for such problems is that the rapid convergence of the series (4) allows numerical calculations to be performed using a finite number of polynomials. Applying the Legendre transformation to (2) yields<sup>26</sup>

$$\hat{\gamma}_n(r_1, r_2) = \frac{4\pi}{2n+1} \int_0^{\infty} dr_3 r_3^2 \hat{c}_n(r_1, r_3) n(r_3) \hat{h}_n(r_3, r_2), \quad (5)$$

where  $\hat{\gamma}_n(r_1, r_2) = \hat{h}_n(r_1, r_2) - \hat{c}_n(r_1, r_2)$  has been introduced for notational convenience. As for planar geometry the spherically inhomogeneous Ornstein-Zernike equation (5) retains a one-dimensional integral. The transformed equation (5) has been used to study the structural properties of a number of model fluids under conditions of spherical inhomogeneity<sup>27</sup>.

A special case of particular interest arises when the external potential is generated by a particle of the fluid fixed at the coordinate origin. In this test-particle limit the one-body density  $n(r)$  is related to the bulk RDF by the Percus identity<sup>28</sup>,  $n(r) = ng(r)$ , and a self-consistent theory for the pair and triplet correlations can be constructed. In order to provide a closed theory the spherically inhomogeneous Ornstein-Zernike equation (5) must be supplemented by an equation for the one-body density  $n(r)$  and a closure relation between  $c(r_1, r_2, x_{12})$  and  $h(r_1, r_2, x_{12})$ . Several exact relations exist which express  $n(r)$  as a functional of the inhomogeneous pair correlation functions. Of particular importance are the first member of the Yvon-Born-Green (YBG) hierarchy<sup>29</sup>, the Triezenberg-Zwanzig (TZ) equation<sup>30</sup> and the Lovett-Mou-Buff-Wertheim (LMBW) equation<sup>31</sup>. We choose to work with the LMBW equation

$$\nabla n(\mathbf{r}_1) = -n(\mathbf{r}_1) \left( \nabla V(\mathbf{r}_1) + \int d\mathbf{r}_2 c(\mathbf{r}_1, \mathbf{r}_2) \nabla n(\mathbf{r}_2) \right), \quad (6)$$

where  $V(\mathbf{r}_1)$  is the external potential in units of  $k_B T$ <sup>32</sup>. In the test-particle limit the external potential is equal to the interparticle pair potential,  $V(\mathbf{r}) = \phi(r)$ , and the LMBW equation reduces to

$$\frac{n'(r_1)}{n(r_1)} = -\phi'(r_1) + \frac{4\pi}{3} \int_0^\infty dr_2 r_2^2 \hat{c}_1(r_1, r_2) n'(r_2), \quad (7)$$

where  $\hat{c}_1(r_1, r_2)$  enters as a result of the angular integrals. The YBG, TZ and LMBW equations all yield exact relations between  $n(r)$  and  $\phi(r)$ , given the exact inhomogeneous correlation functions as input. If  $c(\mathbf{r}_1, \mathbf{r}_2)$  and  $h(\mathbf{r}_1, \mathbf{r}_2)$  are only known approximately, as is always the case in practice, then each of the three equations will yield a different  $n(r)$  for a given  $\phi(r)$ . This structural inconsistency is analogous to the thermodynamic inconsistency familiar from standard integral equation theories based on (1), where each of the three thermodynamic routes (virial, compressibility and energy) yields a different result for the pressure. That an additional inconsistency in the pair correlations occurs between the YBG, TZ and LMBW equations is not surprising and simply reflects that we are working at a higher level in the hierarchy. Our choice to use the LMBW equation is motivated by the

fact that for many situations the derivative  $n'(r)$  decays more rapidly than  $n(r)$ . This is advantageous for numerical implementation as the integral can be discretized over a smaller range.

The exact equations (5) and (7) need to be supplemented by a closure relation between  $c(\mathbf{r}_1, \mathbf{r}_2)$  and  $h(\mathbf{r}_1, \mathbf{r}_2)$ . This closure represents the only approximation within our treatment. Experience with approximate closures of the homogeneous Ornstein-Zernike equation (1) has shown that for statepoints removed from freezing a suitably chosen *local* closure relation between the direct and total correlation function can produce reliable results for the pair structure. We adopt here the same strategy and consider applying the same local closure relations between the inhomogeneous functions as are usually applied between the corresponding homogeneous functions. In the case of the PY and HNC equations such a generalization is natural as both theories follow from well defined diagrammatic resummations. The resummation procedure is not altered by the association of field points in the Mayer cluster diagrams with the spatially varying one-body density  $n(\mathbf{r})$ <sup>16</sup>. Nevertheless, it is not clear that the fortuitous cancellation of errors which can occur when applying a given closure to (1) (e.g. hard-spheres in the PY approximation) will be retained when applying the same closure to (2). Moreover, application of thermodynamically consistent closures at the triplet level does not guarantee improved results, particularly for the description of structure in regions close to the source of inhomogeneity. Despite these potential shortcomings the ultimate assessment of the validity of this approach can only be made from the numerical results, and these are currently very encouraging. Studies of simple model fluids in planar<sup>25</sup> and spherical<sup>27</sup> geometry suggest that significant improvement over standard (homogeneous) integral equation theory can be achieved.

In spherical geometry the formally exact closure relation is given by

$$h(r_1, r_2, x_{12}) + 1 = \exp[-\phi(r_{12}) + h(r_1, r_2, x_{12}) - c(r_1, r_2, x_{12}) + b(r_1, r_2, x_{12})], \quad (8)$$

where  $b(r_1, r_2, x_{12})$  is the bridge function, an intractable sum of elementary diagrams<sup>8</sup>. From among the various improved theories an accurate and computationally efficient approximation for the bridge function is provided by the spherically inhomogeneous generalization of the Verlet-Modified closure<sup>33</sup>

$$b(r_1, r_2, x_{12}) = -\frac{1}{2} \frac{\tau^2(r_1, r_2, x_{12})}{(1 + \alpha \max[\tau(r_1, r_2, x_{12}), 0])}, \quad (9)$$



where the function  $\max[\cdot, \cdot]$  returns the largest of the two arguments and the renormalized indirect correlation function is given by

$$\tau(r_1, r_2, x_{12}) = h(r_1, r_2, x_{12}) - c(r_1, r_2, x_{12}) - \phi_{\text{att}}(r_{12}), \quad (10)$$

where  $\phi_{\text{att}}(r)$  is the attractive part of the pair potential in units of  $k_B T$ . When (9) is applied as a closure to (1) for the hard-sphere system the parameter  $\alpha$  is usually taken to have the value  $0.8^{20,34}$ . The motivation for this choice is that the thermodynamic inconsistency between the compressibility and virial routes to the pressure remains small (within approximately two percent<sup>20</sup>) at all fluid packing fractions. While neglecting possible density dependence of  $\alpha$  only yields approximate thermodynamic consistency, it provides the computational advantage that the integral equation has only to be solved once for a given statepoint. The numerical demands of solving (2) make this an essential requirement for practical application of the inhomogeneous integral equation method. When (9) is applied as a closure to the inhomogeneous Ornstein-Zernike equation (2) the value  $\alpha = 0.8$  is no longer optimal for global thermodynamic consistency. For the hard-sphere system we find  $\alpha = 0.95$  to be a better choice (see the discussion in Section III A below) and it is this value which is employed in all numerical calculations presented in this work. A full discussion of the merits of the closure (9) as applied to (1) can be found in<sup>34</sup>.

Equations (5), (7), (8) and (9) form a closed set which can be solved self-consistently for  $n(r)$ ,  $h(r_1, r_2, x_{12})$  and  $c(r_1, r_2, x_{12})$  for given bulk density  $n$ , temperature and pair potential  $\phi(r)$ . The RDF is easily obtained from the density profile using  $g(r) = n(r)/n$  whereas the bulk triplet-RDF is simply related to the spherically inhomogeneous RDF,  $g(\mathbf{r}_1, \mathbf{r}_2) = h(\mathbf{r}_1, \mathbf{r}_2) + 1$ , by the expression

$$g^{(3)}(r_1, r_2, r_{12}) = g(r_1)g(r_2)g_0(\mathbf{r}_1, \mathbf{r}_2). \quad (11)$$

We employ the notation  $g_0(\mathbf{r}_1, \mathbf{r}_2)$  to indicate that the inhomogeneity is due to a test-particle at the origin. Eq.(11) is essentially the extension of the Percus identity to the next level in the hierarchy of correlation functions. Within this framework the familiar Kirkwood superposition approximation<sup>35</sup> corresponds to  $g_0(\mathbf{r}_1, \mathbf{r}_2) \approx g(r_{12})$ .

The set of equations (5), (7), (8) and (9) were solved self consistently by standard iteration, applying Broyles mixing<sup>8</sup> to both the inhomogeneous pair correlation functions and

the density profile. A mixing parameter between 0.05 and 0.1 was generally found to be sufficient to achieve steady convergence. The convergence rate can be improved by employing the mixing scheme of Ng<sup>36</sup>, but we find that the slight reduction in the number of iterations does not compensate for the additional memory requirements associated with this method. The majority of computation time in numerical solution of the inhomogeneous equations is taken by calculation of the Legendre transforms (3), (4) and the integral (5). In order to minimize computation time we have employed the discrete orthogonal Legendre transform proposed by Attard<sup>26</sup> which is both efficient and prevents the build up of round-off errors during iteration. The mesh for the angular integration (3) is defined by the roots of  $P_n(x)$ , where  $n$  is the highest-order polynomial considered. A cut-off of  $8\sigma$  was found to be sufficient for all calculations presented in the present work. Corrections for the long range tails were made following the suggestions of<sup>37,38</sup> whereby the inhomogeneous functions are replaced by their bulk counterparts far from the source of inhomogeneity. In order to obtain high accuracy solutions we employ a grid spacing  $dr = 0.02$  and between 100 and 140 Legendre polynomials in the sum (4). For hard spheres at packing fractions  $\eta < 0.4$  accurate solutions can be obtained with a coarser mesh. At high density statepoints, for which the liquid is highly structured, it is necessary to work with such a large number of polynomials and a fine grid in order to ensure convergence. For further details of the numerical method we refer the reader to the original work of Attard<sup>26</sup>.

### III. RESULTS

#### A. Hard spheres

We now consider application of equations (5), (7), (8) and (9) to the hard-sphere system at packing fractions close to freezing. In the spirit of the the Verlet-Modified approximation<sup>20</sup> we have determined the value of the parameter  $\alpha$  in (9) by requiring that the pressures obtained from the virial and compressibility equations agree as closely as possible over the entire fluid density range. This is a numerically demanding procedure which requires solution of the integral equation on an  $\eta$ -grid covering the range  $0 < \eta < 0.494$  for each trial value of  $\alpha$ . Numerical accuracy is an issue when calculating the pressure, particularly via the compressibility route, and places limits on the accuracy to which  $\alpha$  can be tuned. We find

that the value  $\alpha = 0.95$  effectively minimizes the difference in the pressures obtained from the two routes, with a residual discrepancy around the one percent level.

Before working close to the freezing transition we first seek to establish the accuracy of our approach at dense fluid statepoints removed from freezing. Monte-Carlo simulations have been performed for the pair and triplet correlations of the hard sphere system at  $\eta = 0.4189$  and serve as a useful benchmark for our theory<sup>39</sup>. We find that at this packing fraction the RDF from the inhomogeneous integral equation theory lies perfectly within the error bars of the simulation data (not shown). As the theory is apparently quasi-exact for the pair correlations we omit this comparison and focus instead on the triplet-RDF for which more significant deviations can be detected. In Figure.2 we show results for the quantity

$$\Gamma(r, s, t) = \frac{g^{(3)}(r, s, t)}{g(r)g(s)g(t)}, \quad (12)$$

for a selection of specific configurations. The quantity  $\Gamma(r, s, t)$  measures deviations from the superposition approximation and is a sensitive indicator of errors in theoretical approximations for the triplet-RDF. Figs.2a and 2b show  $\Gamma(s, s, r)$  as a function of  $r$  for two different values of  $s$  (rolling geometries). Given the high density, the level of agreement between theory and simulation is excellent and essentially all details of the simulation data are faithfully reproduced. It should be noted that use of the test-particle approach in combination with an approximate closure such as (9) leads to a  $g^{(3)}(r, s, t)$  which does not respect the exact particle exchange symmetry expected of this function. We have investigated this discrepancy for each of the configurations shown in Fig.2 and find that the curves differ by at most a few percent, depending upon the location of the test particle in the triangle. This close agreement validates to some extent use of the closure (9) as the approximate particle exchange symmetry is a non-trivial output of the theory. The data shown in Fig.2 were generated with the test particle at the lower left position in the schematic configurations shown. In Figs.2c-2e we consider isosceles triangle configurations for three different triangle base lengths. For  $0 < r < 1.4$  and  $r > 1.8$  the simulation data are well described by the theory. In particular, the increase of the contact value and development of a peak at  $r = 1.9$  in going from 2d to 2e are correctly captured. In the range  $1.4 < r < 1.8$  there are slight discrepancies between theory and simulation as the first minimum is not correctly located. It is reassuring to note that the self-consistently obtained RDF appears insensitive to these fine details and remains accurate, despite modest errors in the underlying triplet structure.

We can thus proceed with confidence to perform calculations closer to freezing.

In Fig.3 we show results for the RDF at packing fractions  $\eta = 0.46, 0.47, 0.48$  and  $0.494$  and compare with the results of molecular dynamics simulations<sup>12</sup>. We concentrate on the range  $1.3 \leq r \leq 2.4$  in order to focus attention on the second peak. At packing fraction  $\eta = 0.46$  the shoulder is just visible in the simulation RDF, marking the onset of local crystalline ordering in the fluid. Remarkably, this behaviour is correctly captured by the present inhomogeneous integral equation theory. Both the shape of the first minimum and the point of inflection which occurs between the first minimum and the second peak are accurately reproduced. As the density is increased the shoulder develops further and by  $\eta = 0.494$  is very pronounced. The present theory describes almost perfectly the evolution of this rich second peak structure as a function of density and captures the characteristic shape of the simulation curves, quite distinct from the triangular form typical of standard approaches based on (1). To the best of our knowledge these findings provide the first convincing evidence that the method of integral equations can indicate the existence of the freezing transition. Moreover, the set of equations (5), (7), (8) and (9) represent the first example of an approximate Ornstein-Zernike closure capable of reproducing from first principles the RDF shoulder. In order to demonstrate the relative insensitivity of our results to changes in the parameter  $\alpha$  we show in the inset to Fig.3 results for values above and below the optimal value  $\alpha = 0.95$ .

Fig.4a and Fig.4b allow a more detailed comparison to be made between theory and simulation, showing the RDF and its derivative at freezing. In Fig.4a we compare the present theory with the result of both simulation and GMSA theory<sup>17</sup> in order to emphasize the inability of such standard integral equation approaches to follow the detailed structure of the simulation curves. In Fig.4b we compare the first derivative  $g'(r)$  from the present theory with simulation and the GMSA. This comparison shows clearly the level of accuracy provided by the inhomogeneous theory. The only slight deviation of the theory from the simulation data occurs in the region in the immediate vicinity of the second peak. This should be contrasted with the GMSA theory which predicts an approximately constant slope over the range  $1.6 < r < 2$ . In addition to the accurate description of the second peak we also find that the first peak and contact value of the RDF are in close agreement with simulation. The resulting virial pressure agrees very favourably with established results for the hard-sphere equation-of-state<sup>40,41</sup>.

## B. Short-range attraction

The simulation studies<sup>6,7</sup> discussed in the introduction provide strong evidence connecting the appearance of a shoulder in the RDF of hard-spheres and hard-disks to the freezing transition. In the previous section we have shown that for hard-spheres the inhomogeneous integral equation theory yields an RDF consistent with this picture. It is therefore tempting to conclude that the appearance of a shoulder in the theoretical RDF can be used as an empirical indicator for locating the freezing transition. However, there remains the possibility that the occurrence of the shoulder and its apparent connection to the onset of freezing may be particular to the hard-sphere (hard-disk) system. We thus seek to investigate the generality of this connection by applying the inhomogeneous theory to a system interacting via a hard-sphere repulsion plus a short-range attraction. For such interaction potentials it is well known that when the range of the attractive interaction becomes sufficiently short-ranged the critical point of the liquid vapour transition becomes metastable with respect to freezing. This is a result of the rapid broadening of the fluid-solid coexistence region as a function of attraction strength which overlaps entirely with the liquid-vapour coexistence region. This novel phase diagram topology thus makes it possible to approach the freezing phase boundary by increasing attraction strength at fixed density. The confirmation of a shoulder in the RDF in the vicinity of this more general freezing phase boundary would considerably strengthen the argument for this empirical freezing indicator.

A well studied pair-potential yielding the required phase diagram topology is that due to Asakura, Oosawa and Vrij<sup>42</sup>. The potential consists of a hard-sphere repulsion plus an attractive tail given by

$$\phi_{\text{AO}}(r) = \eta_p^r \frac{(1+q)^3}{q^3} \left( 1 - \frac{3r}{2(1+q)} + \frac{r^3}{2(1+q)^3} \right) \quad (13)$$

for  $1 < r < 1 + q$  and zero otherwise. The parameter  $q$  sets the range of the potential and the amplitude  $\eta_p^r$  determines the depth of the potential well at contact. This potential has stimulated much interest as it provides a simple approximation to the depletion potential between two hard-sphere colloids in a suspension with added non-adsorbing polymer<sup>43,44</sup>. In this context  $\eta_p^r$  is the packing fraction of polymer coils in a reservoir attached to the system. For the purpose of the present work  $\eta_p^r$  may simply be regarded as a parameter determining the strength of the attractive interaction. The potential (13) is convenient because there exist simulation data for the phase boundaries in the  $(\eta_p^r, \eta_c)$  plane for several values of the range

parameter  $q$ . In Fig.5 we show the simulation phase diagram for  $q = 0.4^{44}$ . For this value of  $q$  the liquid-vapour phase boundary is metastable, albeit weakly, with respect to freezing and the potential is only moderately short-range. For very short-range potentials ( $q < 0.2$ ) resolution of the high and narrow first peak in the RDF requires a spatial grid finer than the  $dr = 0.02$  presently employed and leads to unacceptable computational demands. The choice  $q = 0.4$  thus represents a reasonable compromise, being both numerically tractable and displaying the desired phase diagram topology.

In order to analyse the structural predictions of the inhomogeneous theory for the potential (13) we approach the freezing boundary along two distinct paths in the phase diagram. The statepoints for which we present detailed results are indicated in Fig.5. We consider first the packing fraction  $\eta = 0.35$  and investigate the RDF as a function of increasing  $\eta_p^r$ , approaching the freezing boundary along a vertical path in the phase diagram. In Fig.6 we show the RDF in the vicinity of the second peak for four different statepoints. At statepoint (a) the RDF is simply that of hard-spheres ( $\eta_p^r = 0$ ) and displays the expected oscillatory structure. As the attraction is increased (statepoint (b)) there is a notable increase in structure over that of pure hard-spheres. The shifting of the first minimum and second peak to smaller separations reflects the increased interparticle attraction which tends to pull the next-nearest-neighbours closer to the central particle. Nevertheless, the results for statepoints (a) and (b) can still be well reproduced by standard integral equation closures. At statepoint (c) additional fine structure not captured by standard theories becomes evident in the second peak and a marginal point of inflection occurs. For slightly stronger attraction (statepoint (d)) this structure develops into a distinct shoulder, reminiscent of that seen close to the freezing transition of pure hard-spheres. The development of the shoulder between statepoints (c) and (d) is consistent with the broadened freezing transition found in simulation, as shown in Fig.5, and occurs over a relatively narrow range of attraction strengths ( $0.43 < \eta_p^r < 0.47$ ). It may be inferred that the appearance of this attraction-driven shoulder reflects the existence of underlying precursor structures in the intermediate density fluid. In Fig.7 we consider approaching the freezing boundary at the lower packing fraction  $\eta = 0.2$ . Increasing the attraction strength from statepoint (e) to (g) we observe the expected increase in fluid structure. Statepoint (h) lies just below the freezing phase boundary and exhibits the onset of a weak shoulder which develops as the attraction strength is further increased to statepoint (i). In accord with the findings for  $\eta = 0.35$  the onset of the shoulder occurs over

a relatively narrow range of attraction strength and is consistent with the location of the simulation phase boundary. For this lower packing fraction the shoulder is less pronounced and is shifted to slightly smaller separations, indicating the decreased statistical weight of the locally ordered regions within the fluid. The striking correlation between the onset of the shoulder and the simulation phase boundary lead us to conclude that the RDF shoulder is a genuine freezing indicator for a broad class of model interaction potentials and not simply an artifact of the hard-sphere fluid at high density.

#### IV. DISCUSSION

In this paper we have demonstrated that inhomogeneous integral equation theory provides a highly accurate description of the hard-sphere fluid RDF at densities up to the freezing transition. In agreement with simulation the theory displays the onset of a shoulder in the second peak which is associated with the formation of local crystalline regions in the dense fluid. When applied to a system of hard-spheres plus a short-range attraction the inhomogeneous theory predicts the development of a shoulder as a function of attraction strength consistent with the simulation freezing phase boundary. That the inhomogeneous integral equation theory is capable of capturing these subtle effects demonstrates the accuracy with which local packing constraints are treated. The fact that the present theory acknowledges the existence of the freezing boundary is a significant development beyond standard integral equation closures and validates the significant increase in computational resources required for numerical solution of the equations. Although the present study is restricted to three dimensional systems we anticipate that application of the inhomogeneous theory in two dimensions would lead to broadly similar conclusions.

For the purpose of this work we have focussed on fluid state structure in the vicinity of freezing. However, the inhomogeneous theory is also capable of a description of the liquid-vapour phase transition which occurs for systems with longer-range attraction than that considered here. For  $q > 0.45$  the potential (13) exhibits a stable liquid-vapour transition. Preliminary calculations for range parameter  $q = 0.6$  display a large increase in the compressibility along a locus of points in the phase diagram consistent with the simulation liquid-vapour phase boundary<sup>44</sup>. We therefore feel justified in claiming the theory developed in this work to be the first example of an Ornstein-Zernike closure sensitive to both

the second-order liquid vapour transition and the first-order freezing transition. This goes a step beyond existing integral equation approaches which at best display a line in the phase diagram upon which the compressibility either diverges (spinodal) or the theory breaks down (no-solutions boundary)<sup>10</sup> and which show no indication of freezing. Of particular interest would be the characterization of the spinodal for the present theory and the determination of the critical exponents which, given the nature of the closure, may be non-classical<sup>45</sup>.

## Acknowledgements

We acknowledge the transregio SFB TR6 for financial support. We thank E. Lange for stimulating discussions and for providing molecular dynamics data.

- 
- <sup>1</sup> B.J. Alder and T.E. Wainwright, *J.Chem.Phys.* **27** 1208 (1957)
- <sup>2</sup> W.G. Hoover and F.H. Ree, *J.Chem.Phys.* **49** 3609 (1968)
- <sup>3</sup> R. Evans, in *Fundamentals of inhomogeneous fluids*, edited by D. Henderson (Dekker, New York, 1992), p.85.
- <sup>4</sup> P. Tarazona, *Physica A* **306** 243 (2002)
- <sup>5</sup> R. Roth, R. Evans, A. Lang and G. Kahl, *J.Phys.Cond.Mat.* **14** 12063 (2002)
- <sup>6</sup> T.M. Truskett *et al*, *Phys.Rev.E.* **58** 3083 (1998)
- <sup>7</sup> B. O'Malley and I. Snook, *J.Chem.Phys.* **123** 054511 (2005)
- <sup>8</sup> J-P. Hansen and I.R. McDonald, *Theory of simple liquids* (Academic, London, 1986)
- <sup>9</sup> C. Caccamo, *Physics.Rep.* **274** 1 (1996)
- <sup>10</sup> J.M. Brader, *Int.J.Thermophys.* **27** 394 (2006)
- <sup>11</sup> Empirical studies of the hard-sphere shoulder have been performed using extrapolations of simulation data, see S. Labík and A. Malijevský, *Mol.Phys.* **67** 431 (1989), A. Malijevský, S. Labík and W.R. Smith, *ibid.* **72** 193 (1991)
- <sup>12</sup> E. Lange (private communication)
- <sup>13</sup> The solid phase radial distribution function shown in Figure.1 was generated using the Kincaid-Weis fit to the simulation data, J.M. Kincaid and J.J. Weis, *Mol.Phys.* **34** 931 (1977)



- <sup>14</sup> J.K. Percus and G.J. Yevick, Phys.Rev. **110** 1 (1958), G. Stell, Physica **29** 517 (1963), M.S. Wertheim, Phys.Rev.Lett. **10** 321 (1963), E. Thiele, J.Chem.Phys. **38** 1959 (1963)
- <sup>15</sup> J.M.J. van Leeuwen, J. Groeneveld and J. deBoer, Physica **25** 792 (1959), E. Meeron, J.Math.Phys. **1** 192 (1960), T. Morita, Prog.Theor.Phys. **23** 829 (1960), G.S. Rushbrooke, Physica **26** 259 (1960), L. Verlet, Il Nuovo Cimento **18** 77 (1960)
- <sup>16</sup> For a review of diagrammatic techniques see G. Stell, in *Equilibrium theory of classical fluids* (H.L. Frisch and J.L. Lebowitz eds.) Benjamin, New York (1964)
- <sup>17</sup> E. Waisman, Mol.Phys. **25** 45 (1973)
- <sup>18</sup> G.A. Martynov and G.N. Sarkisov, Mol.Phys. **49** 1495 (1983)
- <sup>19</sup> P. Ballone, G. Pastore, G. Galli and D. Gazzillo, Mol.Phys. **59** 275 (1986)
- <sup>20</sup> L. Verlet, Mol.Phys. **41** 183 (1980)
- <sup>21</sup> F.J. Rogers and D.A. Young, Phys.Rev.A **30** 999 (1984)
- <sup>22</sup> Y. Rosenfeld and N.W. Ashcroft, Phys.Rev.A **20** 1208 (1979)
- <sup>23</sup> We have performed numerical calculations for all of the approximate closures mentioned in the text and find the shoulder to be absent in all cases.
- <sup>24</sup> S. Sokołowski, J.Chem.Phys. **73** 3507 (1980), R.M. Nieminen and N.W. Ashcroft, Phys.Rev.A **24** 560 (1981)
- <sup>25</sup> R. Kjellander and S. Marcelja, J.Chem.Phys. **82** 2122 (1985), R.A. McGough and M.D. Miller, Phys.Rev.A **34** 457 (1986), M. Plischke and D. Henderson, J.Chem.Phys. **84** 2846 (1986), I. Omelyan, F. Hirata and A. Kovalenko, PCCP **7** 4132 (2005).
- <sup>26</sup> P. Attard, J.Chem.Phys. **91** 3072 (1989)
- <sup>27</sup> A. Malijevsky, S. Sokołowski and T. Zientarski, J. Chem. Phys. **125** 114505 (2006), E. Lomba, S. Jorge and M. Álvarez, Phys.Rev.E **63** 011203 (2000), D. Henderson and S. Sokołowski, J.Chem.Phys. **103** 7541 (1995), D. Henderson and S. Sokołowski, J.Chem.Phys. **104** 2971 (1996), P. Attard, J.Chem.Phys. **91** 3083 (1989)
- <sup>28</sup> J.K. Percus, in *Equilibrium theory of classical fluids* (H.L. Frisch and J.L. Lebowitz eds.) Benjamin, New York (1964)
- <sup>29</sup> J. Yvon, *Actualités scientifiques et industrielles* (Hermann & Cie., Paris, 1935), M. Born and H.S. Green, Proc.Roy.Soc.A (London) **188**, 10 (1946)
- <sup>30</sup> D.G. Triezenberg and R. Zwanzig, Phys.Rev.Lett. **28** 1183 (1972)
- <sup>31</sup> R. Lovett, C.Y. Mou and F.P. Buff, J.Chem.Phys. **65** 570 (1976), M.S. Wertheim J.Chem.Phys.

**65** 2377 (1976)

- <sup>32</sup> Another potentially useful exact relation between the density derivative of the RDF and the integrated triplet-RDF is Eq.(61) from the review by G.S. Rushbrooke, in *Physics of simple liquids* (H.N.V. Temperly, J.S. Rowlinson and G.S. Rushbrooke) North-Holland, Amsterdam chapter.2 (1968)
- <sup>33</sup> The original Verlet-Modified closure<sup>20</sup> was developed for hard spheres but proved less successful for systems with attractive interactions. The improved version (9) employed in this work was subsequently proposed in<sup>34</sup> to correct these failings.
- <sup>34</sup> N. Choudhury and S.K. Ghosh, *J.Chem.Phys.* **116** 8517 (2002)
- <sup>35</sup> J.G. Kirkwood, *J.Chem.Phys.* **3** 300 (1935)
- <sup>36</sup> K.C. Ng *J.Chem.Phys.* **61** 2680 (1974)
- <sup>37</sup> P. Attard, *J.Chem.Phys.* **95** 4471 (1991)
- <sup>38</sup> M. Fushiki, *Mol.Phys.* **74** 307 (1991)
- <sup>39</sup> E.A. Müller and K.E. Gubbins, *Mol.Phys.* **80** 91 (1993)
- <sup>40</sup> A. Malijevsky and J. Veverka, *PCCP* **1** 4267 (1999)
- <sup>41</sup> A useful review of the various hard-sphere equations-of-state can be found in A. Mulero, C. Galán and F. Cuadros, *PCCP* **3** 4991 (2001)
- <sup>42</sup> S. Asakura and F. Oosawa, *J.Chem.Phys.* **22** 1255 (1955), S. Asakura and F. Oosawa, *J.Polym.Sci.* **33** 183 (1958), A. Vrij, *Pure Appl.Chem.* **48** 471 (1976)
- <sup>43</sup> A.P. Gast, C.K. Hall and W.B. Russel, *J.Colloid Interface Sci.* **96** 251 (1983)
- <sup>44</sup> M. Dijkstra, J.M. Brader and R. Evans, *J.Phys.Cond.Mat.* **11** 10079 (1999)
- <sup>45</sup> A. Parola and L. Reatto, *Il Nuovo Cimento* **6 D** 215 (1985)

Figure 1. Hard-sphere RDF from computer simulation at freezing,  $\eta = 0.494$  (full line) and at the melting point  $\eta = 0.545$  (dashed line). The inset focuses on the shoulder in the second peak of the simulation RDF at freezing (full line). The broken line is the result of GMSA theory and is representative of the inability of standard integral equation theories to capture the shoulder.

Figure 2. Comparison of the results of inhomogeneous integral equation theory with the simulation results of Müller and Gubbins<sup>39</sup> for the quantity  $\Gamma(r, s, t)$  for  $\eta = 0.8\pi/6 \approx 0.4189$ . The geometries are schematically shown in each figure. The separation  $r$  is indicated by a line in each case. (a) and (b) are rolling geometries at  $s = t = 1.0$  and  $s = t = 1.1$ , respectively. (c)-(e) are isocetes triangle configurations with  $s = r$  and the base length of the triangle fixed at  $t = 1.1, 1.3$  and  $1.5$ , respectively.

Figure 3. The RDF of hard-spheres for packing fractions  $\eta = 0.46, 0.47, 0.48$  and  $0.494$  (from bottem to top). For clarity the data for  $\eta = 0.47, 0.48$  and  $0.494$  have been shifted vertically by  $0.2, 0.4$  and  $0.6$ , respectively. Solid lines are the results of the inhomogeneous integral equation theory. Open circles are from molecular dynamics simulations<sup>12</sup>. The inset shows the sensitivity of the second peak to changes in the parameter  $\alpha$  for  $\eta = 0.494$ . Results are shown for the optimal value  $\alpha = 0.95$  (solid line),  $\alpha = 1.05$  (broken line) and  $\alpha = 0.85$  (dotted line).

Figure 4. Comparison of the inhomogeneous integral equation theory (solid line) for  $\eta = 0.494$  with simulation data (open circles)<sup>12</sup> and the GMSA theory (dashed line)<sup>17</sup>. (a) and (b) show the RDF and the first derivative of the RDF, respectively.

Figure 5. The simulation phase diagram calculated using the Asakura-Oosawa pair potential (13) in the  $(\eta, \eta_p^r)$  plane<sup>44</sup>. The range of attraction is  $q = 0.4$  and  $\eta_p^r$  represents the strength of the attraction. The solid line is the fluid-solid phase boundary and the dashed line indicates the (metastable) liquid-vapour transition. Squares labelled a-d and circles labelled e-i mark the state points for which we present detailed results.

Figure 6. The RDF from inhomogeneous integral equation theory for the statepoints labelled a-d in Fig.5. In each case the packing fraction  $\eta = 0.35$ . Statepoint (a)  $\eta_p^r = 0$  (dotted line), (b)  $\eta_p^r = 0.3$  (dot-dashed line), (c)  $\eta_p^r = 0.43$  (broken line) and (d)  $\eta_p^r = 0.47$  (full line). The development of the shoulder is consistent with the simulation freezing phase boundary presented in Fig.5.

Figure 7. As for Fig.6 but for the statepoints labelled e-i in Fig.5. In each case the packing fraction  $\eta = 0.20$ . Statepoint (e)  $\eta_p^r = 0$  (dotted line), (f)  $\eta_p^r = 0.2$  (dot-dashed line), (g)  $\eta_p^r = 0.4$  (double dot-dashed line), (h)  $\eta_p^r = 0.45$  (broken line) and (i)  $\eta_p^r = 0.47$  (full line).

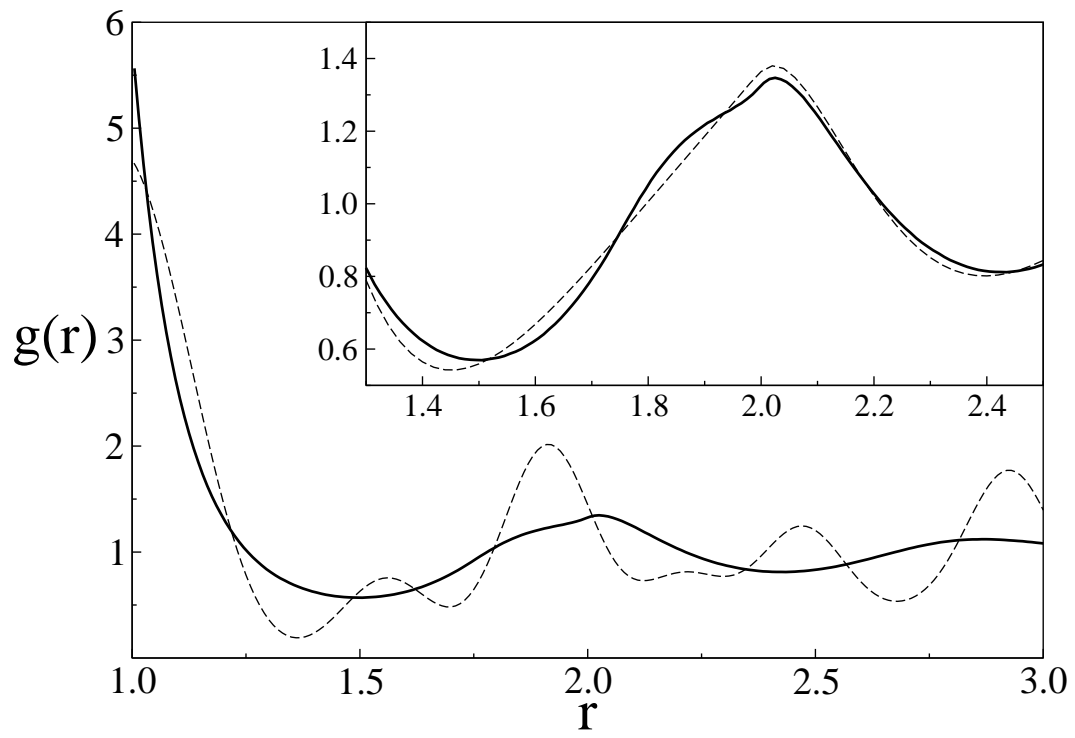


FIG. 1:

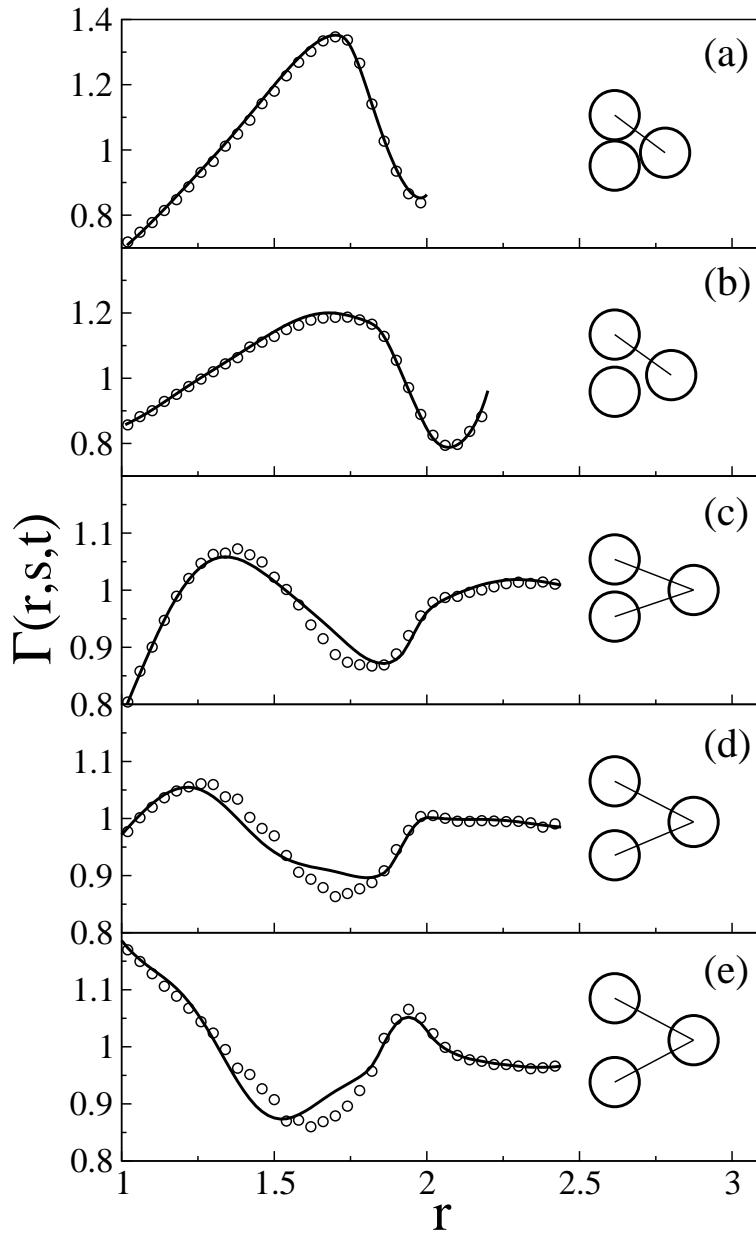


FIG. 2:

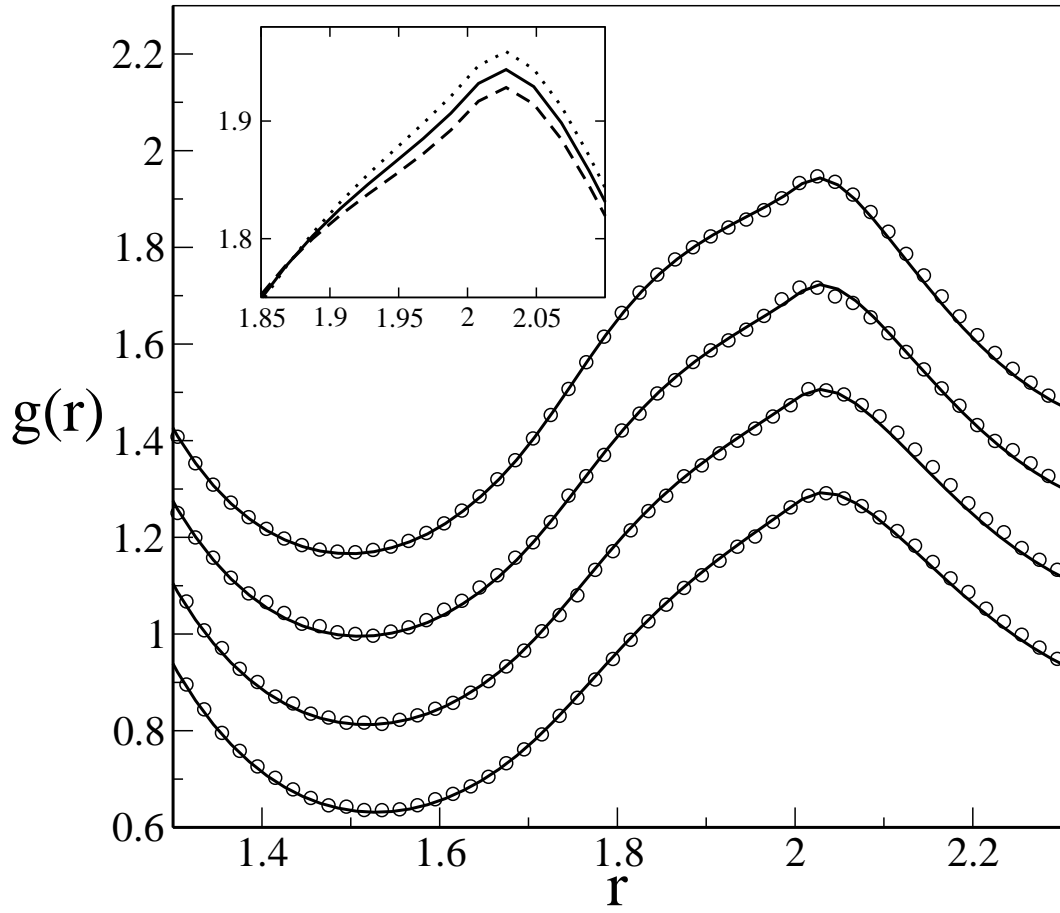


FIG. 3:

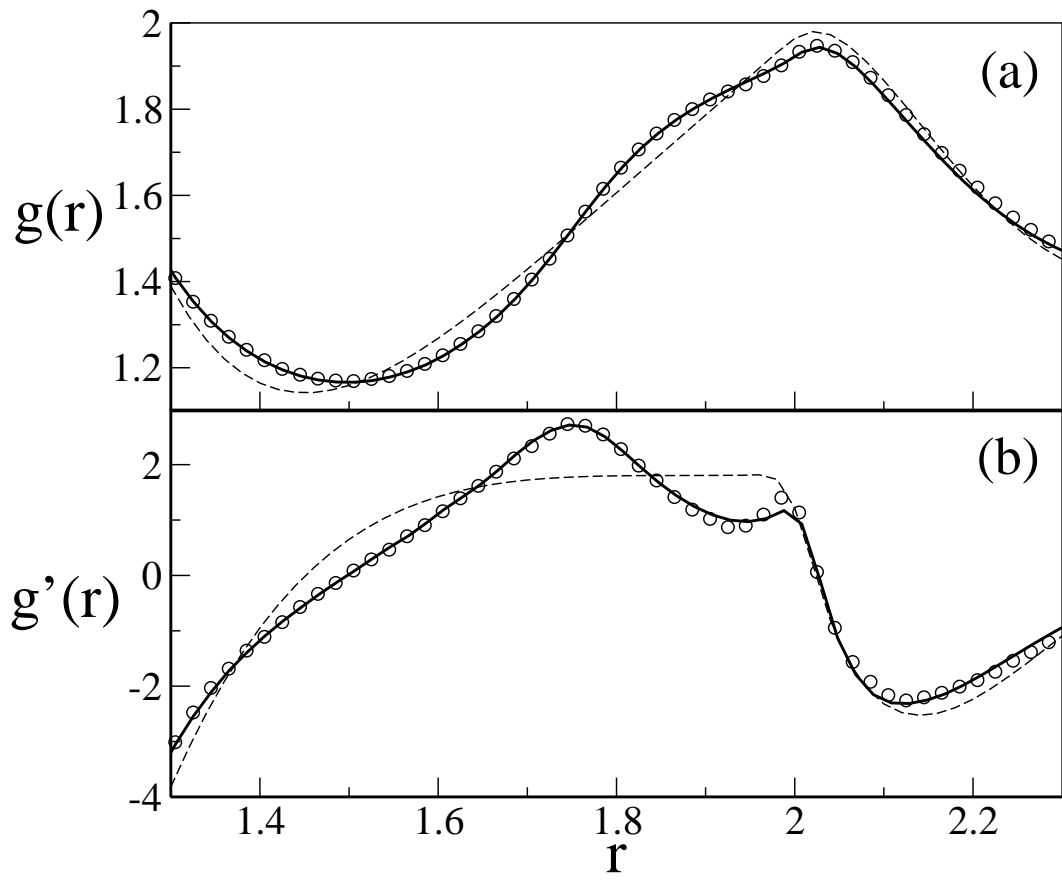


FIG. 4:



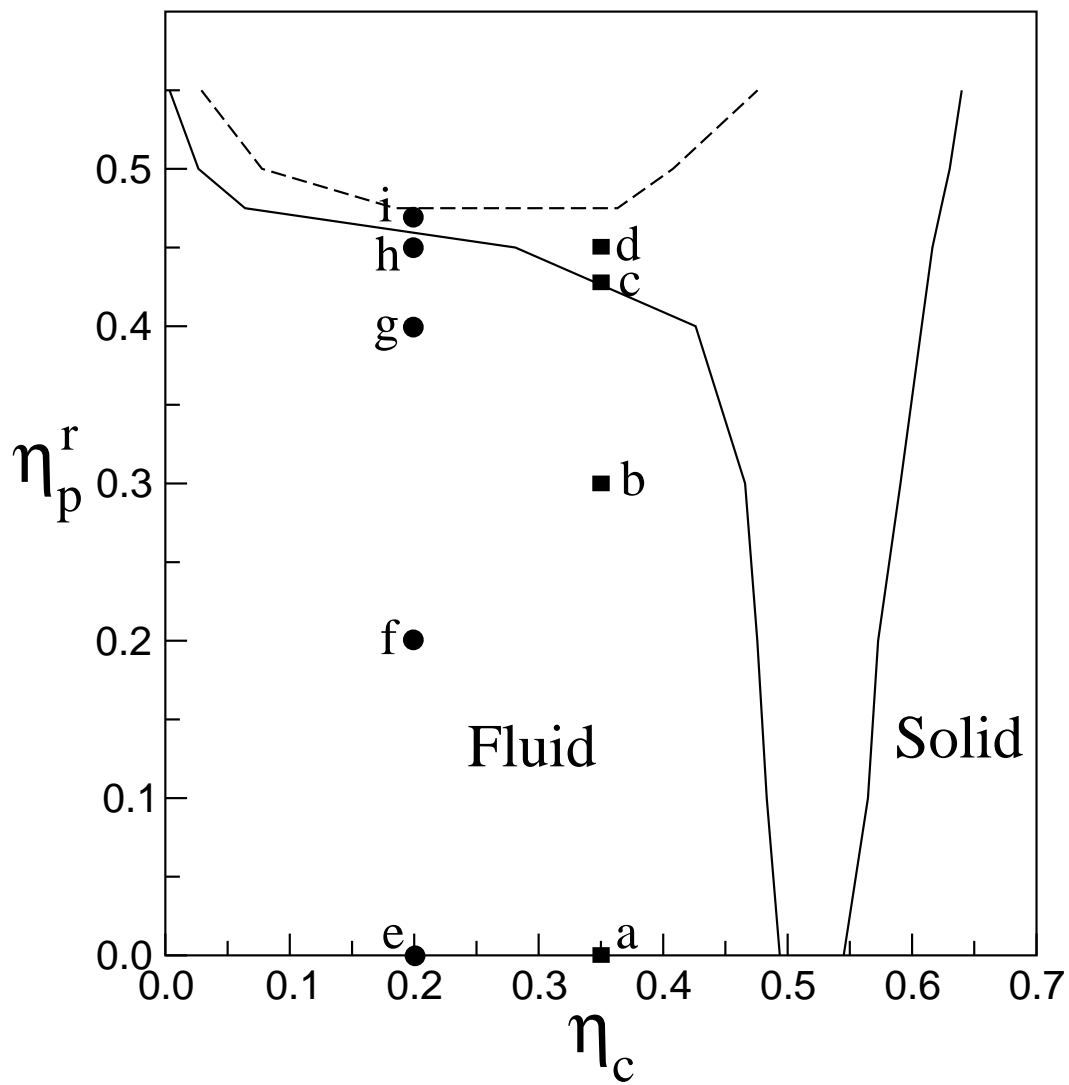


FIG. 5:

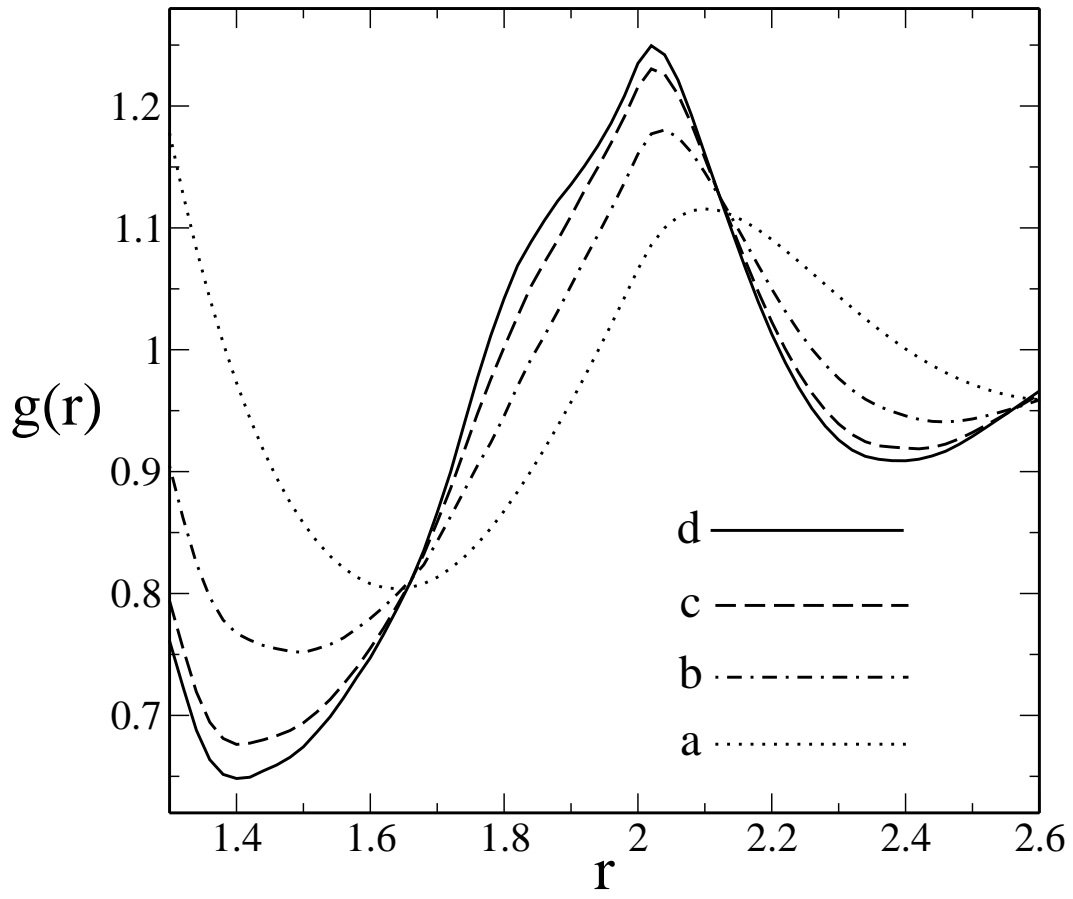


FIG. 6:

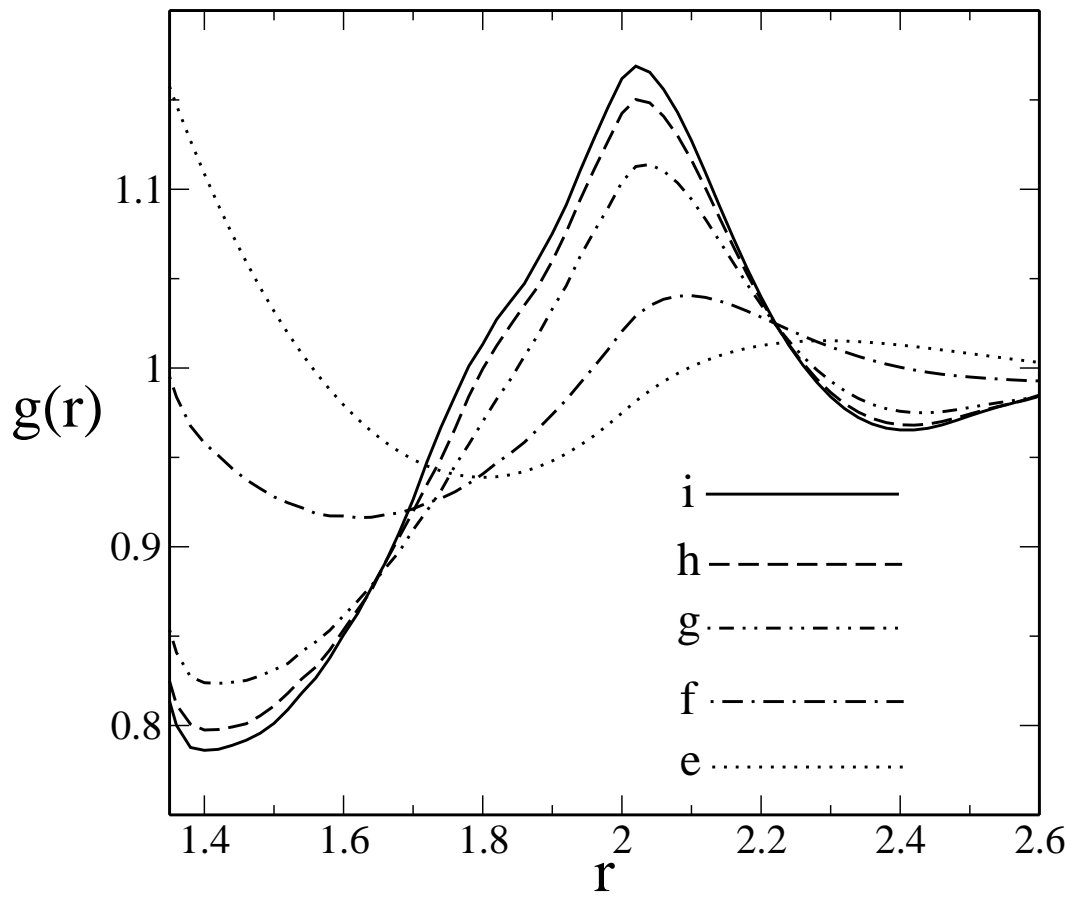


FIG. 7: